Available online at www.sciencedirect.com

ScienceDirect

Procedia Structural Integrity 28 (2020) 266–278

Structural Integrity Procedia

www.elsevier.com/locate/procedia

1st Virtual European Conference on Fracture

Inhomogeneous FEM model for fracture simulation of aluminosilicate glass

Zhen Wang[a,b], Tao Suo[a], Andrea Manes[b*]

[a]School of Aeronautics, Northwestern Polytechnical University, Xi'an 710072, Shaanxi, PR China
[b]Politecnico di Milano, Department of Mechanical Engineering, Milan 20156, Italy

Abstract

Aluminosilicate glass possesses excellent mechanical and functional properties. It combines relatively low density, high hardness and strength in compression. However, the very low tensile strength and inherent brittleness are main concerns to its application. Due to the presence of microheterogeneity and randomly distributed surface flaws, the mechanical strength and failure mechanisms of silicate glasses varies considerably, even for the same glass products. In the present work, inhomogeneous FEM models were proposed and utilized to simulate the discrete failure strength and replicate the multiple crack patterns of aluminosilicate glass. Special attention was paid to the quasi-static three-point bending and ballistic impact loading conditions in this paper. The results from experiments and simulations were compared in detail and show that both the failure strength and fracture modes can be reproduced properly via the proposed numerical models both for three-point bending tests and for ballistic impact conditions. In the latter both the predicted residual velocity of projectile and the fragmentation behavior of glass tiles from the inhomogeneous FEM method show better matching than the homogeneous models.

Keywords: aluminosilicate glass; brittle failure; inhomogeneous model; fracture mode

1. Introduction

Glass products and structures gained wide acceptance over the centuries due to their excellent mechanical and functional properties. (Varshneya, 2018) They are used as aircraft windshields, bullet proof armors, hurricane resist glass windows, as well as electronic touch screen. These glass structures usually undertake complex and changing loading conditions. The brittleness and low tensile strength are two main drawbacks to the structural application of

* Corresponding author. Tel.: ++39-02 23998630; fax: ++39-02 23998263.
E-mail address: andrea.manes@polimi.it

10.1016/j.prostr.2020.10.032

glass components, which may result in sudden failure of structures and are potentially life-threatening to human beings. The mechanical strength and failure types of silicate glasses varies considerably due to the microheterogeneity and randomly distributed surface flaws. Many efforts such as chemical strengthening (Zhen et al., 2018) and surface HF etching (Wang, Guan, et al., 2020) have been made to reduce the severity of surface flaws and make glass sheets less vulnerable to failure. It is thus an essential and challenging work to predict the failure range and conduct the safety assessment for glass components.

Among all the numerical methods, finite element method (FEM) is the most widely used and efficient one. It is a well-established method that can be used in engineering design and evaluation at large scales. In recent years, FEM models were also utilized to analyze the probabilistic failure of brittle materials. Osnes et al (Osnes, Børvik, & Hopperstad, 2018; Osnes, Hopperstad, & Børvik, 2020) proposed a glass strength prediction model as a function of its geometry, boundary conditions and loading situation. This model reproduced the fracture behavior of glass plates under both quasi-static and dynamic loading conditions well. Sapozhnikov et al (Ignatova, Sapozhnikov, & Dolganina, 2017; Sapozhnikov, Kudryavtsev, & Dolganina, 2015) developed microstructural and voxel-based FEM models to assess the deformation and failure of porous ceramics. Stochastic pore distribution in ceramics was represented by assigning different material properties for different elements randomly in the numerical approach. The experimental and numerical results agreed quite well with both piston-on-ring bending and ballistic tests. The complex crack propagation behavior of quasi-brittle materials considering random heterogeneous fracture properties was also realized by FE coupled to a cohesive element's method.(Su, Yang, & Liu, 2010; Yang, Su, Chen, & Liu, 2009) It has been illustrated that the heterogeneous model is capable of predicting realistic complex crack propagation and accurate load-carrying capacity with much improved mesh objectivity for assessing structural reliability and calculating the characteristic strength of materials for structural design.

In the present work, an inhomogeneous FEM method was used to replicate the probabilistic failure strength and crack patterns of aluminosilicate glass by the commercial software LS-DYNA. The numerical results were compared with the observations from three-point bending and ballistic impact tests. Both the reproduced failure strength and fracture properties are more realistic when compared with the results form homogeneous models. The proposed method is a simple but effective numerical tool for assessing structural reliability of brittle materials and can be easily applied to large scale engineering structures. The article is divided into four sections. Section 2 provides a brief introduction of the experimental tests. Section 3 introduces the proposed numerical model together with the parameter calibration process. Subsequently the simulation results of the three-point bending and ballistic impact tests are discussed and compared with the experimental observations in section 4. The last section provides some brief conclusions of this paper.

2. Experimental tests

Three-point bending and ballistic impact tests were conducted on aluminosilicate glass (Zhen et al., 2018). The dimensional size of the specimens for the two different tests is the same, as shown in Figure 1. For the three-point bending tests, the length l, width b and thickness h of specimens were 120mm, 19mm and 8mm respectively. The flexural strength can be calculated by

$$\sigma_f = \frac{3Pl}{2bh^2} \tag{1}$$

where P represents the maximum loading capacity of the specimens. The loading speed was fixed at 0.2 mm/min during the tests, which can be regarded as quasi-static loading condition.

For ballistic impact tests, a gas gun was utilized to launch steel bullets. The weight of a C-45 steel flat-nosed projectile is 12.4±0.1g with impact velocities of 84m/s and 139m/s. Two aluminum bars were used to support the glass tile at the same place identical to the support used in the three-point bending tests. (Wang, Li, et al., 2020) It is worth noting that high-speed cameras were used to capture the crack initiation, propagation and the specimens fracture process for all the tests.

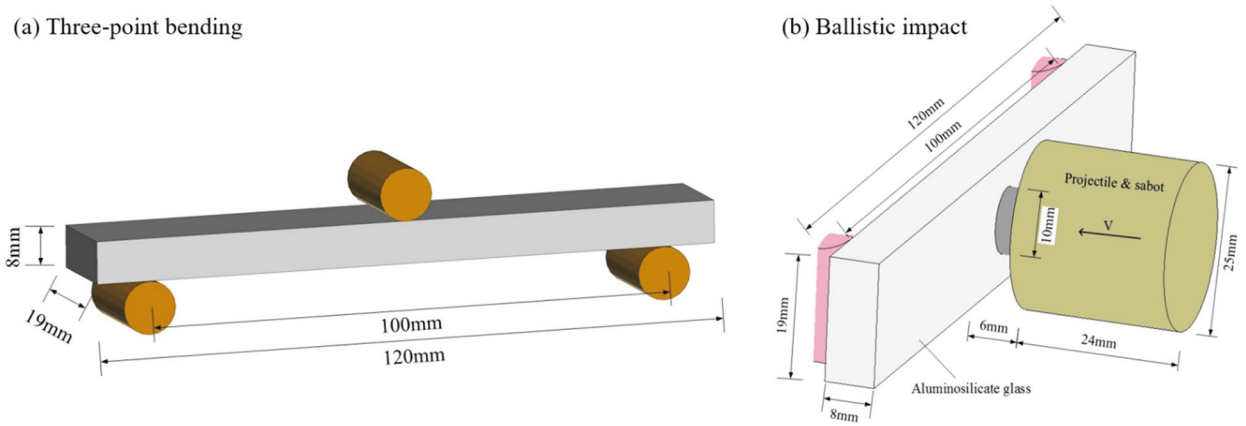

Fig. 1. Schematic graph of experimental tests on aluminosilicate glass

3. Numerical method

3.1 model description

For all the numerical simulations in this work, full-size models were used with a fixed mesh size of 0.5 mm, which has already been validated by a mesh size sensitivity analysis. JH-2 constitutive model (Holmquist, Johnson, Lopatin, Grady, & Hertel Jr, 1995) composed of a polynomial equation of state (EOS), a normalized strength model and a damage evolution relationship was adopted to reproduce the brittle fracture and ballistic impact response of aluminosilicate glass. This material model has been proven to efficiently reproduce and predict the fracture and failure behavior of brittle materials, especially in dynamic loading conditions (Lahiri, Shaw, & Ramachandra, 2019; Toussaint & Polyzois, 2019). The model parameters for aluminosilicate glass were obtained by mechanical tests on specimens on material coupons as well as some literature data. This process was described in detail in our recent work (Wang, Li, et al., 2020) and the calibrated material constants are listed in Table 1. As for the material failure and fracture simulation, element erosion and adaptive FEM elements to SPH particles technique were adopted. When the erosion criterion is satisfied, one failed element adaptively transforms into one SPH particle instead of just being deleted. The SPH particle will inherit all the same mechanical properties as the converted solid elements, including mass, kinematic variables, and constitutive properties. This technique is very suitable for fracture analysis of brittle materials, especially in some complex loading conditions like tool-rock penetration (Mardalizad, Saksala, Manes, & Giglio, 2020) and high-speed impact (Bresciani, Manes, Romano, Iavarone, & Giglio, 2016).

Table 1. JH-2 model constants for aluminosilicate glass (Wang, Li, et al., 2020)

Parameter	Value	Parameter	Value
ρ_0 (kg•m^{-3})	2545.62	B	0.2
γ	0.22	M	1
E (GPa)	75.13	K_1 (GPa)	44.72
σ_{HEL} (GPa)	5.95	K_2 (GPa)	-67.45
P_{HEL} (GPa)	3.07	K_3 (GPa)	141.60
$\sigma_{t,max}$ (MPa)	44.25	β	1
A	0.93	D_1	0.043
N	0.76	D_2	0.85
C	0.036		

In a three-point bending loading condition, the loaded surface of the specimen undergoes compression, while the opposite surface undergoes tension. Due to the high compression strength and the much lower tensile strength of silicate glass, the tensile surface will fail once the applied stress reaches its limitation. The comparison of the flexural strength between experiments and homogeneous FEM numerical simulation is shown in Figure 2 (a). The experimental data shows that the strength of brittle materials differs a lot even between specimens of the same batch. A deterministic regular FEM model can only provide an average strength but cannot represent the strength distribution range. Actually, the simulated tensile strength of aluminosilicate glass is controlled by the maximum hydrostatic tensile strength $\sigma_{t,max}$ in the JH-2 material model. The parameter $\sigma_{t,max}$ was set as 5MPa, 20MPa, 40MPa, 100MPa, 200MPa, 300MPa to simulate the flexural strength of glass specimens, as shown in Figure 2 (b). There is a nearly linear relation between the simulated flexural strength and $\sigma_{t,max}$. The calibrated value of $\sigma_{t,max}$ for aluminosilicate glass is 44.25MPa (Table 1) from Brazilian disc tensile tests. The simulated flexural strength estimated by the homogeneous FEM model is 82MPa, corresponding to the average flexural strength from experimental tests. As for the simulated flexural failure mode of the FEM simulation, the elements beneath the loading spot are exposed to the largest tensile strength and a straight crack appeared to divide the specimen into two parts, just as expected from this model. However, this failure mode is not realistic compared with experimental observations. During experiments, cracks don't always initiate from the same places due to the random distribution of surface flaws. Also, the crack propagation paths are usually not in a straight line because of the material microheterogeneity property. Crack deflection and bifurcation are very common phenomenon for the failure process of brittle materials. All of these failure modes cannot be reproduced by regular homogeneous FEM models.

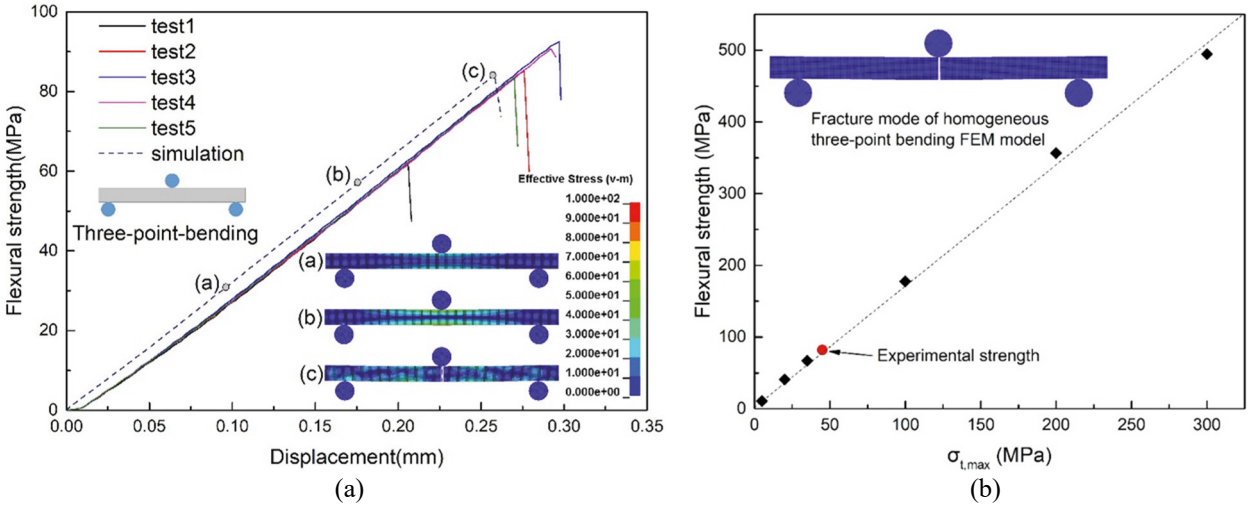

Fig. 2. (a) Comparison of flexural strength between experiments and homogeneous FEM numerical simulation; (b) effect of $\sigma_{t,max}$ on the flexural strength of glass specimens

Following the stochastic concept in (Ignatova et al., 2017; Sapozhnikov et al., 2015), inhomogeneous FEM models were built by setting stochastic material properties to different elements. In Figure. 3 (a), randomly distributed elements with low strength were used on the surface of the specimen to represent the randomly distributed flaws. Thereby some discrete brittle failure behavior of aluminosilicate glass can be reproduced and cracks do not always initiate from the middle part of the specimens (Figure 2). However, the numerical simulation still fails to predict the phenomenon of crack deflection and bifurcation. Figure 3 (b) improved the inhomogeneous model by setting defect elements randomly in the whole specimens, but the fracture mode from this method is still not comparable to experimental observations. Another drawback of this model is that the stiffness of the specimen decreases with the softening and failure of weak elements, which is not the case for the brittle failure process of aluminosilicate glass.

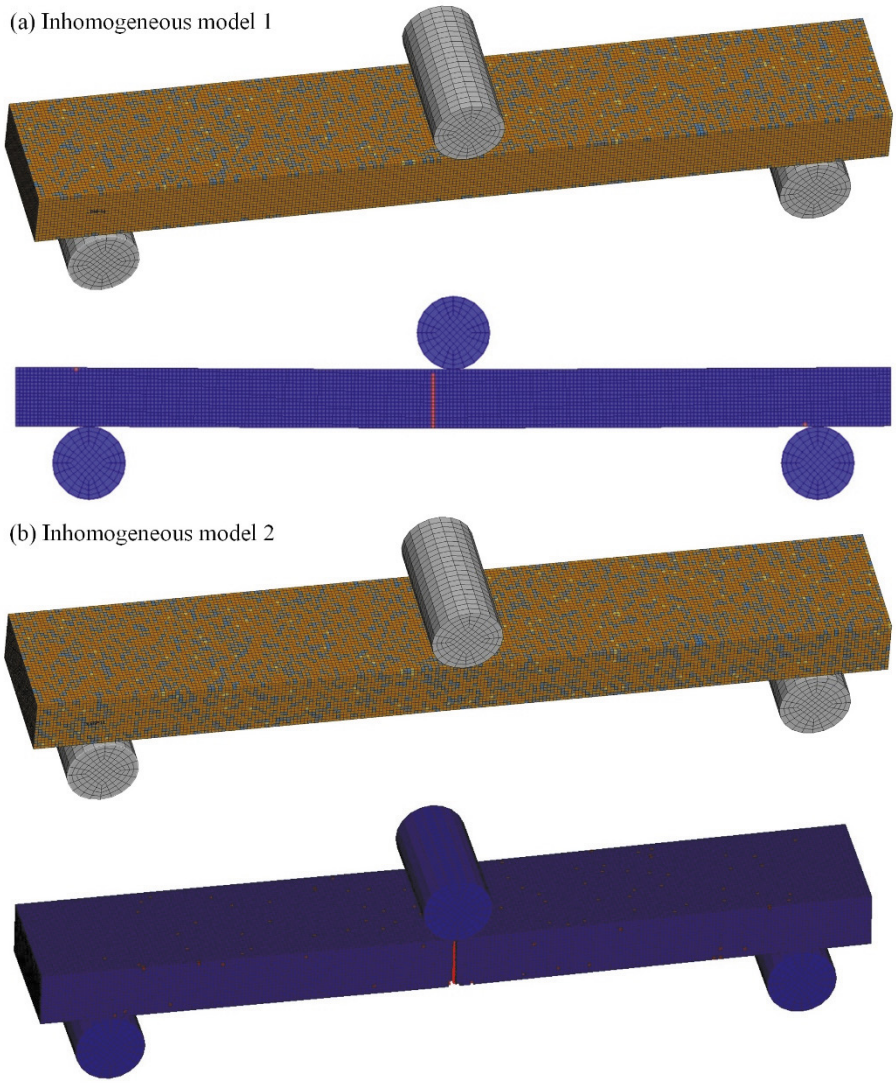

Figure 3. Inhomogeneous FEM models and corresponding simulation results

To better represent the random property of silicate glass, a modified inhomogeneous FEM model was developed, as shown in Figure 4. In this model, the elements were randomly assigned by different material models by following a proportion, shown by different colors in the graph. Part A makes up the majority of the specimen volume with a normal strength material model, which is obtained from the average strength of the numerical results. Part B represents the stronger part of the specimen with a stronger material strength model, corresponding to the microheterogeneity property of silicate glass. When cracks propagate to the front of part B elements, crack deflection and branching may occur as in a realistic situation. Part C is assigned with weak tensile strength to simulate the effect of randomly distributed surface flaws, which affect the crack initiation spots and mechanical strength of specimens remarkably. The elements of part C only exist in the surface of the numerical model, just like the flaws in the surface of the specimens. This model is supposed to mimic the fracture and fragmentation behavior of silicate glass in a more realistic fashion.

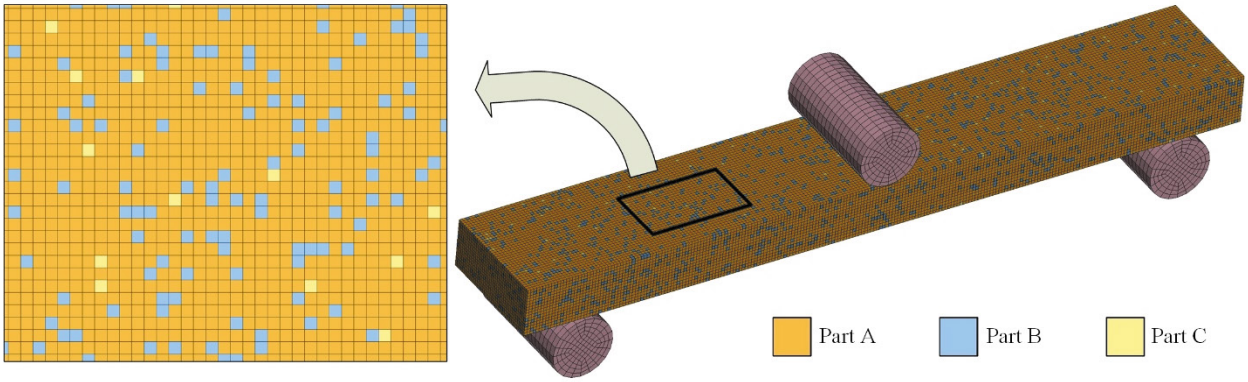

Figure 4. Modified inhomogeneous FEM model

3.2 Parameters calibration

To better represent the mechanical behavior of aluminosilicate glass, a proper setting of the volume fraction and $\sigma_{t,max}$ of parts B and C is necessary. The influence of part B was investigated firstly, where the volume fraction and

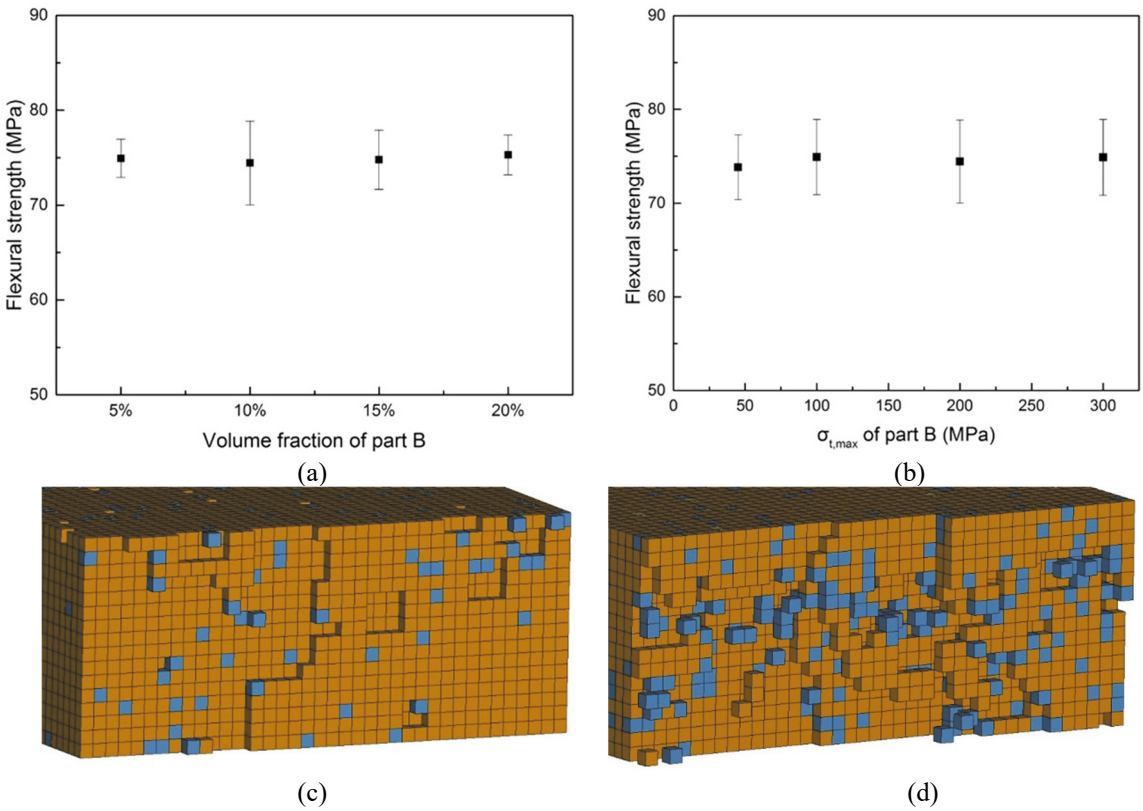

Figure 5. (a) Effect of volume fraction of part B on the simulated flexural strength; (a) effect of $\sigma_{t,max}$ of part B on the simulated flexural strength; (c) typical fracture surface with 5% volume fraction of part B ($\sigma_{t,max}$ of part B is 200MPa); (c) typical fracture surface with 10% volume fraction of part B ($\sigma_{t,max}$ of part B is 200MPa).

$\sigma_{t,max}$ of part C was fixed at 1% and 5MPa here. It is worth noting that 10 specimens were built randomly for the same parameters and the average strength and standard deviation were plotted in the figures below. The effect of the volume fraction of part B on the flexural strength is shown in Figure 5 (a). The $\sigma_{t,max}$ of part B was fixed at 200MPa in this condition. Different volume fractions (5%, 10%, 15%, 20%) of part B were used to generate FEM models. The average flexural strength increases slightly with the increase of the volume fraction of the stronger elements in this range. A 10% volume fraction can reproduce the diversity of the flexural strength better. The effect of $\sigma_{t,max}$ of part B is shown in Figure 5 (b), where the volume fraction of part B was fixed at 10% for convenience of comparison. The flexural strength of the specimens increases with $\sigma_{t,max}$ of part B slightly. However, the fracture behavior differs a lot for different settings of part B. Figure 5 (c) and (d) show typical fracture surfaces with a volume fraction of part B set as 5% and 10%. With 5% of stronger elements, the fracture surface is much flatter without many curves or bifurcations and the random fracture property cannot be reproduced properly. When the volume fraction of part B increases to 10%, a more realistic fracture surface can be obtained. The cracks curved when facing the stronger elements. Considering both the flexural strength and fracture behavior of the numerical results, the 10% volume fraction and $\sigma_{t,max}$ as 200MPa of part B were used in this work.

As for the volume fraction and $\sigma_{t,max}$ of part C, the same approach was used to investigate the parametric influences. In this case, all the simulations were conducted with the 10% volume fraction and $\sigma_{t,max}$ 200MPa of part B. Figure 6 (a) shows the effect of the volume fraction of part C on the simulated flexural strength. $\sigma_{t,max}$ of part C was set as 5MPa for all the three cases (0.5%, 1%, 2%). It can be seen that the average flexural strength decreases with the increase of the volume fraction of weak elements, corresponding to the surface flaws of aluminosilicate glass. The effect of $\sigma_{t,max}$ of part C is shown in Figure 6 (b) and a fixed volume fraction 1% is used here. When the maximum hydrostatic tensile strength of part C increases to 20MPa from 5MPa, the average flexural strength is nearly constant, but it clearly increases when $\sigma_{t,max}$ increases to 35MPa. Figure 6 (c) shows the maximum principle stress in the specimen's tensile surface during loading process. Stress concentration appears around the weak elements (part C). In this way, cracks will initiate from the most severe places due to the random distribution of weak elements.

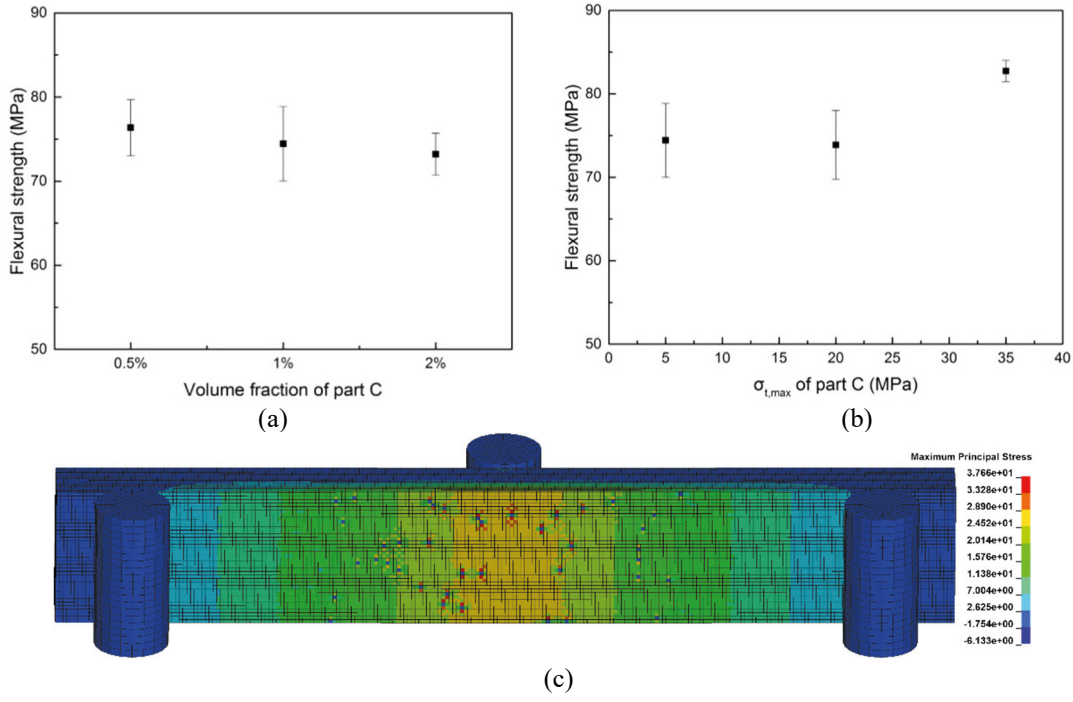

Fig. 6. (a) Effect of volume fraction of part C on the simulated flexural strength; (b) effect of $\sigma_{t,max}$ of part C on the simulated flexural strength; (c) stress concentration around the elements of part C.

4. Results and discussion

4.1 Three-point bending

The simulated flexural strength values by the inhomogeneous models are shown in Figure 7. Different numerical models have been built stochastically: they exploit the same calibrated parameters stated in section 3.2 but the distribution of Part A, B and C is stochastically obtained. Since the models are inhomogeneous with randomly distributed elements (part B and part C shown in Figure 4) with different material properties, the strength values for different models are different. Ten models were used for the simulation and the numerical strength values remain very well in the range of the experimental results. It is worth noting that the stiffness of the numerical specimens declined slightly when weak elements (part C) failed during the loading process. However, the elements of part C only exist on the surface of the specimens and account for a tiny volume fraction, so this effect can be neglected in this process.

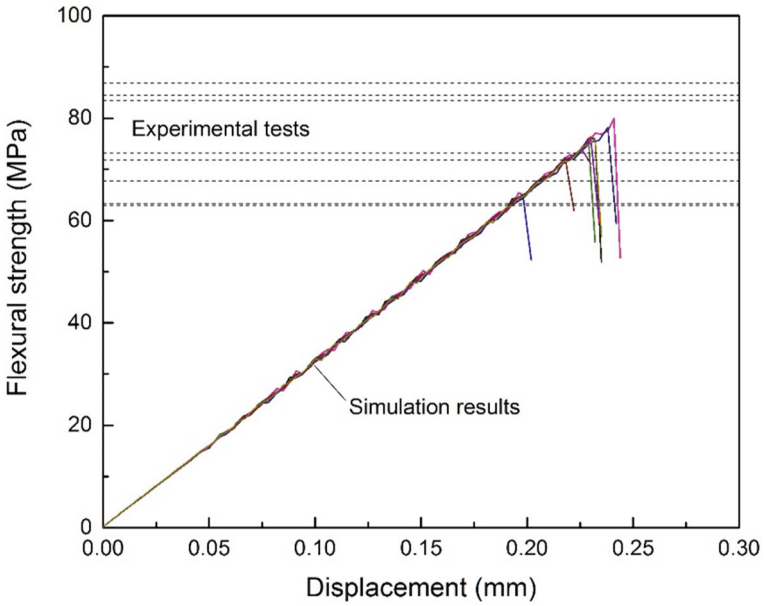

Fig. 7. Comparison between simulated flexural strength with experimental results

During three-point bending tests, a high-speed camera was utilized to record the fracture modes of glass specimens. The typical fracture and failure modes of glass specimens are shown in Figure 8, with different specimens exhibiting different failure modes. The high-speed image in Figure 8 (a) not only shows that there is not one single crack but a small damage region around the indenter but shows also that the cracks formed are not straight but curved during the propagation process. For the second failure mode shown in Figure 8 (b), except for the main crack in the middle of the specimen, stopped cracks also appeared near the main crack. The last picture shows that cracks not only initiate from the middle of the specimens, but also from other spots sometimes due to the random surface flaws. Normal homogeneous FEM models are unable to reproduce any of the failure modes proposed here. However, the discrete failure property and failure modes can be well replicated via inhomogeneous FEM models in this paper. Selected simulation results (from statistical models) are also shown below to compare with experimental observations. This numerical method is simple but very effective for the assessment of brittle material strength and failure analysis. It can be also used for large scale engineering structures in the field of structural reliability and design.

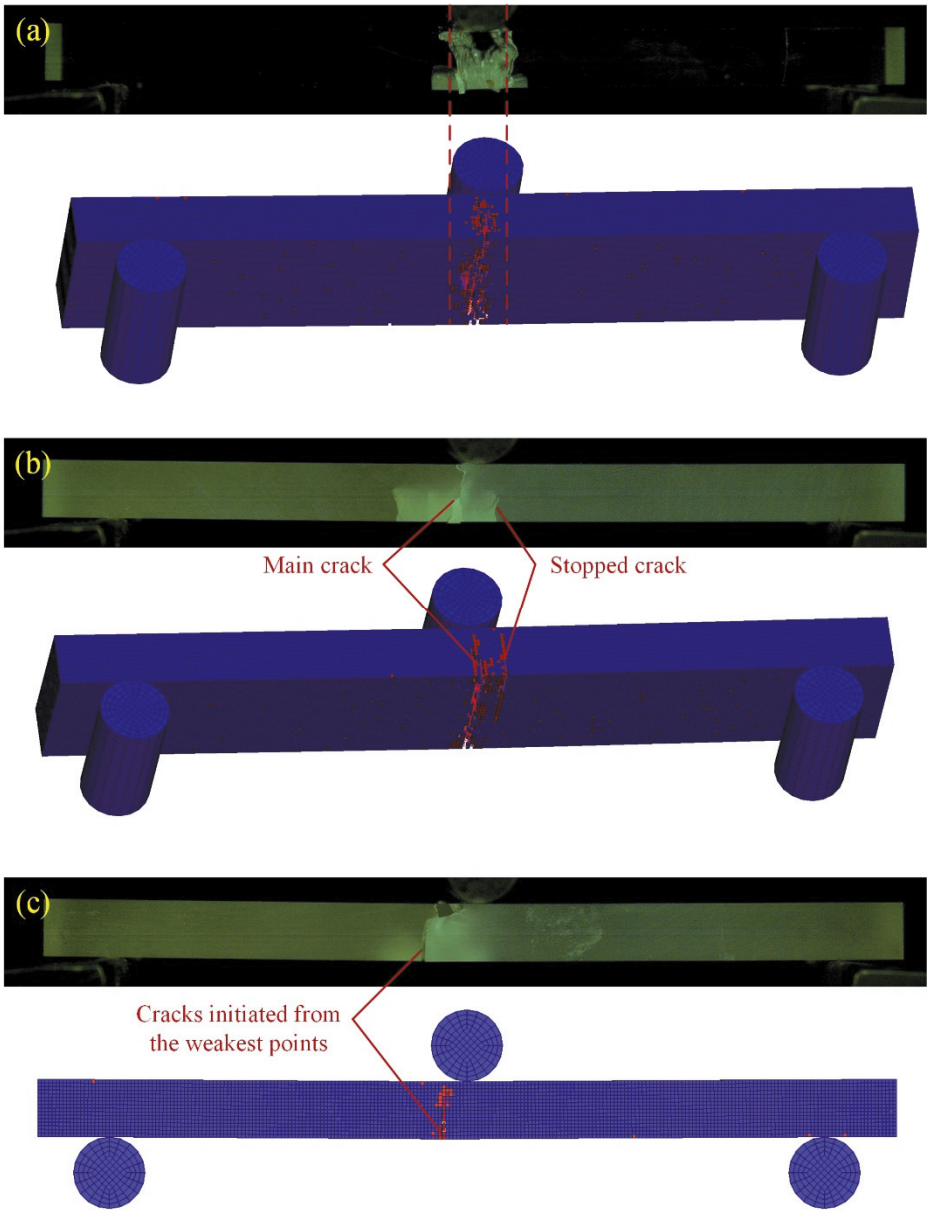

Fig. 8. Comparison of different failure models

4.2 Ballistic impact

The Inhomogeneous method was also used to replicate the fracture and fragmentation behavior of aluminosilicate glass tiles penetrated by steel bullets. The FEM model is shown in Figure 9. Identical size glass tiles were used in the impact and in the three-point bending tests. Two aluminum bars were used to support the glass specimen during the tests. The C-45 steel bullet was covered by a plastic sabot to improve the trajectory during tests. Also, an ultra-high-speed camera was used to record the failure process and crack propagation during tests. A more detailed description about this experiment can be found in (Wang, Li, et al., 2020).

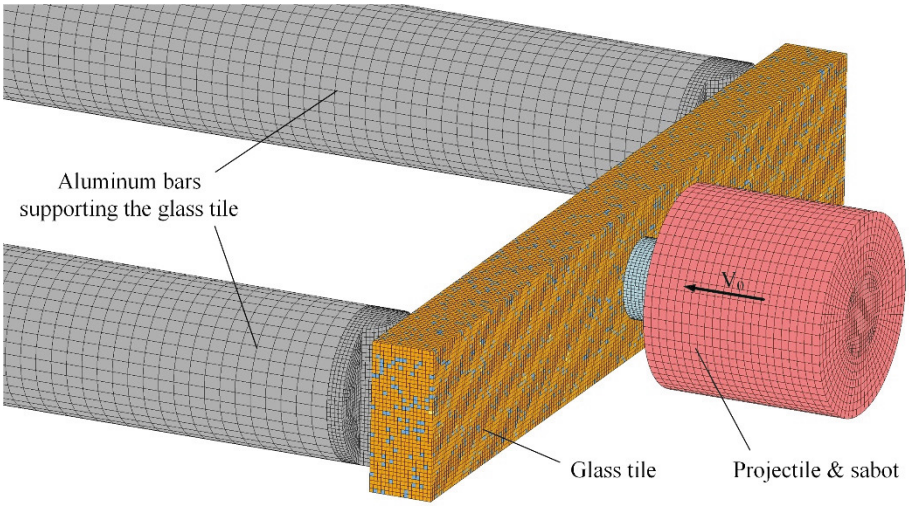

Figure 9. Inhomogeneous FEM model for ballistic impact tests

Two impact tests were conducted on aluminosilicate glass tiles with impact velocities of 84m/s and 139m/s. The residual speeds for each test are 66m/s and 127m/s respectively. The predicted residual speed of the steel projectiles for both the homogeneous and inhomogeneous models are shown in Figure 10. Five stochastic inhomogeneous FEM models were utilized for the simulation for each condition. The velocity history is nearly the same for different inhomogeneous models for the dynamic loading conditions. Both the homogeneous and inhomogeneous models can predict the residual speed of projectiles very well. Even for the higher impact velocity of 139m/s the predicted residual speed from inhomogeneous models (127m/s) is more accurate than the homogeneous FEM model (123m/s).

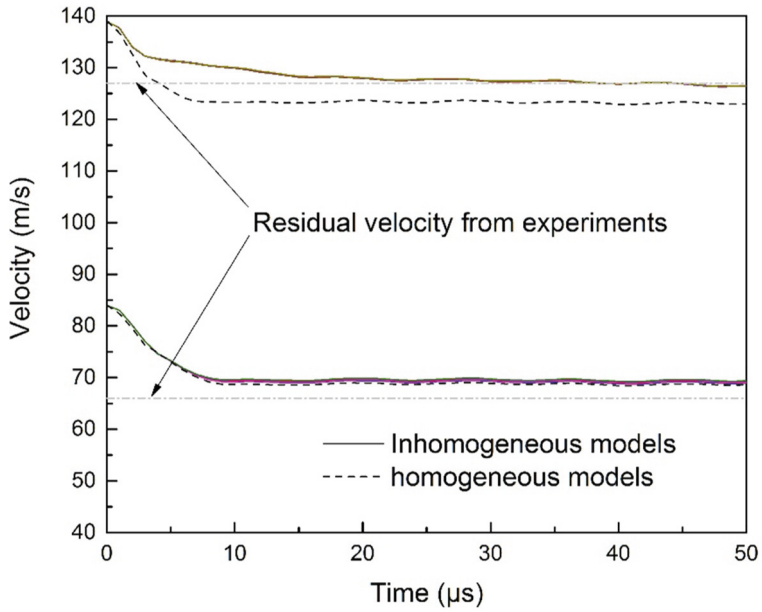

Fig. 10. Comparison of the projectile residual velocity between experiments and the simulation

The observed and numerically reproduced fragmentation behavior of glass tile impacted by a flat-nosed projectile is shown in Figure 11. For flat-nosed projectiles, the surface of the bullet end contacted the glass tile surface at the beginning of the impact process. Cracks initiated from the impact side of the tile at 2μs, shown as the white area in the image. At 4μs, the compression wave in the glass tiles reached the rear surface of the tile and was reflected as a tensile wave. Damage appeared at the rear end of the glass tile due to the low tensile strength of glass. The front and rear cracks interact with each other and formed a damage area around the impact site at 6μs. This process from 0-6μs can be predicted very well by both the homogeneous and inhomogeneous models. However, the inhomogeneous method provided better predictions of the cracks further away from the impact area, while the damage and crack density simulated by the homogeneous model is much lower than the experimental observations. There is usually a main crack in the center spot for the homogeneous model. The inhomogeneous models allow multiple crack initiations, deflection and bifurcation, which are visible in the high-speed images at 18μs and 66μs.

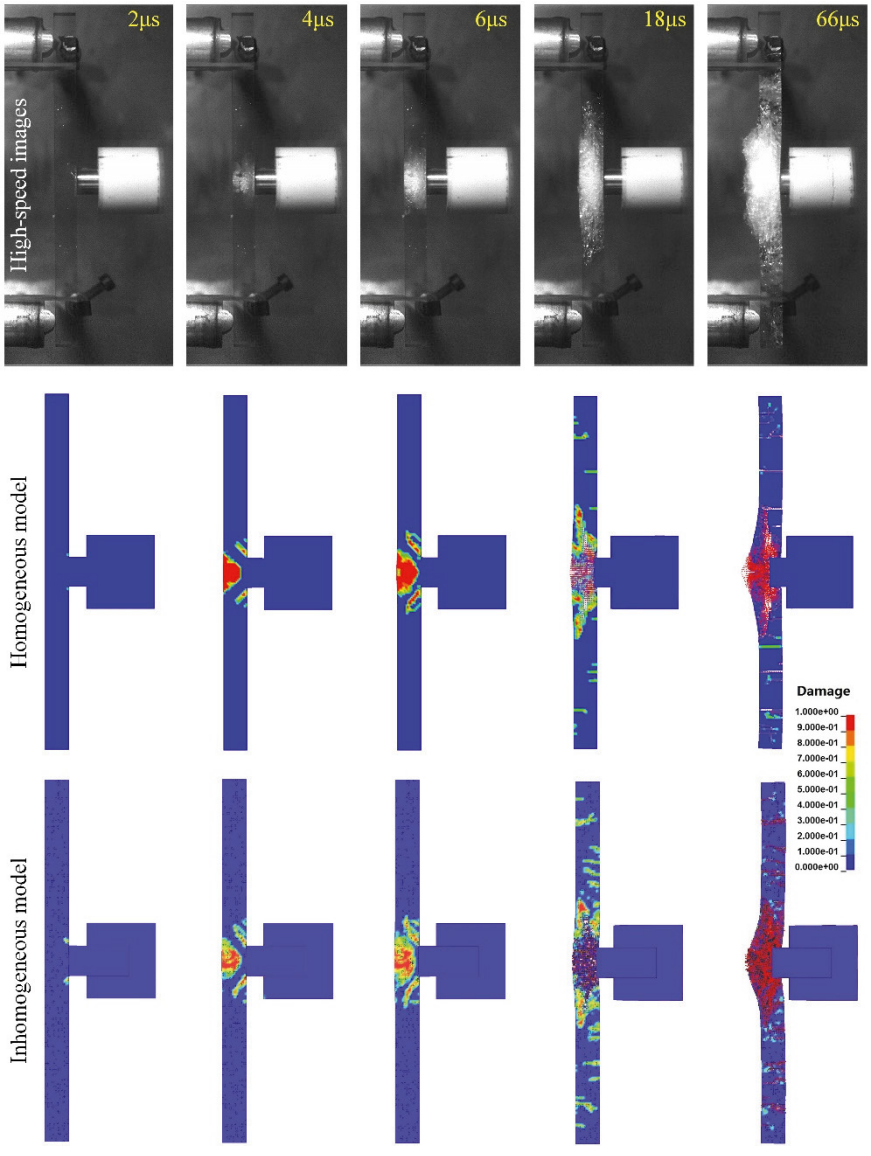

Fig. 11. Fragmentation behavior of impacted glass tile

A detailed fragmentation and crack analysis can be seen in Figure 12. The cracked specimens after penetration can be divided into three regions. Region I is the directly impacted region which is an area of a circular shape full of cracks. The circular shape of the damage area can be better represented by the proposed inhomogeneous model. For the crack area Region II and Region III, main cracks were reproduced in the homogeneous model without many crack deflections. Also, the predicted cracks area was smaller than the experimental observations. The inhomogeneous method shows a better capacity to describe this behavior and both the crack morphology and damage area size compares well with experimental observations.

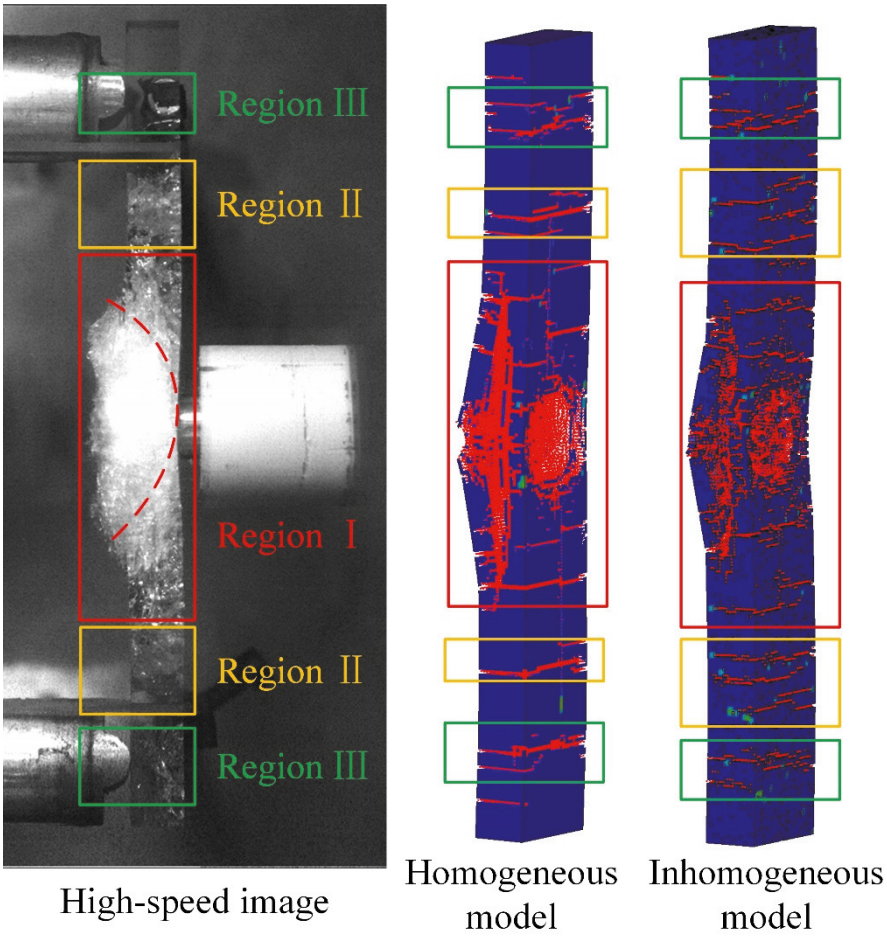

Figure 12. A detailed comparison of fracture models of glass specimens

5. Conclusions

A computational FEM modeling method has been developed to simulate the brittle failure and fragmentation behavior of aluminosilicate glass with random heterogeneous fracture properties. The inhomogeneous FEM models consider randomly distributed surface flaws and the microheterogeneity property by using randomly distributed elements with different mechanical properties. The heterogeneous model is capable of predicting realistic complex crack propagation modes and accurate load-carrying capacity for aluminosilicate glass in three-point bending tests. This method also shows potential for the simulation of ballistic impact problems, where the predicted projectile speed and fragmentation type of glass tiles are more comparable to experimental observations compared to the homogeneous

FEM method. This proposed method can be also extended to more complex loading conditions as well as other brittle materials such as ceramics, rock, concrete, etc. Overall, the proposed approach in the present work shows the powerful potential to numerically reproduce stochastic brittle failure behaviors.

Acknowledgement

The author, Zhen Wang, thanks the Chinese Scholarship Council for its financial support (CSC, No. 201906290120) to conduct scientific research at Politecnico di Milano, Italy. Dr. Massimo Fossati at Politecnico di Milano is acknowledged for his help to guarantee the remote research activities during the epidemic.

References

Bresciani, L., Manes, A., Romano, T., Iavarone, P., & Giglio, M. (2016). Numerical modelling to reproduce fragmentation of a tungsten heavy alloy projectile impacting a ceramic tile: Adaptive solid mesh to the SPH technique and the cohesive law. *International Journal of Impact Engineering, 87*, 3-13.

Holmquist, T. J., Johnson, G. R., Lopatin, C., Grady, D., & Hertel Jr, E. (1995). High strain rate properties and constitutive modeling of glass: Sandia National Labs., Albuquerque, NM (United States).

Ignatova, A., Sapozhnikov, S., & Dolganina, N. Y. (2017). Development of microstructural and voxel based models of deformation and failure of the porous ceramics for assessment of ballistic performance. *International Journal of Mechanical Sciences, 131*, 672-682.

Lahiri, S. K., Shaw, A., & Ramachandra, L. (2019). On performance of different material models in predicting response of ceramics under high velocity impact. *International Journal of Solids and Structures, 176*, 96-107.

Mardalizad, A., Saksala, T., Manes, A., & Giglio, M. (2020). Numerical modeling of the tool-rock penetration process using FEM coupled with SPH technique. *Journal of Petroleum Science and Engineering, 189*, 107008.

Osnes, K., Børvik, T., & Hopperstad, O. S. (2018). Testing and modelling of annealed float glass under quasi-static and dynamic loading. *Engineering fracture mechanics, 201*, 107-129.

Osnes, K., Hopperstad, O. S., & Børvik, T. (2020). Rate dependent fracture of monolithic and laminated glass: Experiments and simulations. *Engineering Structures, 212*, 110516.

Sapozhnikov, S., Kudryavtsev, O., & Dolganina, N. Y. (2015). Experimental and numerical estimation of strength and fragmentation of different porosity alumina ceramics. *Materials & Design, 88*, 1042-1048.

Su, X., Yang, Z., & Liu, G. (2010). Monte Carlo simulation of complex cohesive fracture in random heterogeneous quasi-brittle materials: A 3D study. *International Journal of Solids and Structures, 47*(17), 2336-2345.

Toussaint, G., & Polyzois, I. (2019). Steel spheres impact on alumina ceramic tiles: Experiments and finite element simulations. *International Journal of Applied Ceramic Technology, 16*(6), 2131-2152.

Varshneya, A. K. (2018). Stronger glass products: Lessons learned and yet to be learned. *International Journal of Applied Glass Science, 9*(2), 140-155.

Wang, Z., Guan, T., Ren, T., Wang, H., Suo, T., Li, Y., Iwamoto, T., Wang, X., Wang, Y., Gao, G. (2020). Effect of normal scratch load and HF etching on the mechanical behavior of annealed and chemically strengthened aluminosilicate glass. *Ceramics International, 46*(4), 4813-4823.

Wang, Z., Li, Y., Ma, D., Li, Y., Suo, T., & Manes, A. (2020). Experimental and Numerical Investigation on the Ballistic Performance of Aluminosilicate Glass with Different Nosed Projectiles. *Submitted to International Journal of Impact Engineering*.

Yang, Z., Su, X., Chen, J., & Liu, G. (2009). Monte Carlo simulation of complex cohesive fracture in random heterogeneous quasi-brittle materials. *International Journal of Solids and Structures, 46*(17), 3222-3234.

Zhen, W., Zhenbiao, H., Tao, S., Fenghua, Z., Yulong, L., Sheikh, M. Z., Xiang, W., Yinmao, W. (2018). A comparative study on the effect of loading speed and surface scratches on the flexural strength of aluminosilicate glass: annealed vs. chemically strengthened. *Ceramics International, 44*(10), 11239-11256.